

Published in final edited form as:

*Medchemcomm.* 2014 June 1; 5(6): 826–830. doi:10.1039/C4MD00126E.

## Design, Synthesis, and Evaluation of 4- and 5-Substituted *o*-(Octanesulfonamido)benzoic Acids as Inhibitors of Glycerol-3-Phosphate Acyltransferase

Victor K. Outlaw<sup>a</sup>, Edward A. Wydysh<sup>a</sup>, Aravinda Vadlamudi<sup>b</sup>, Susan M. Medghalchi<sup>b</sup>, and Craig A. Townsend<sup>a</sup>

<sup>a</sup>Department of Chemistry, The Johns Hopkins University, Remsen Hall, 3400 N. Charles Street, Baltimore, MD 21218, USA

<sup>b</sup>FASGEN, Inc., UMB Research Park, Building One, 800 W. Baltimore St., Suite 150, Baltimore, MD 21201, USA

### Abstract

Despite a rising demand for anti-obesity therapeutics, few effective pharmacological options are clinically available that target the synthesis and accumulation of body fat. Moderate inhibition of mammalian glycerol-3-phosphate acyltransferase (GPAT) with 2-(alkanesulfonamido)benzoic acids has recently been described *in vitro*, accompanied by promising weight loss *in vivo*. *In silico* docking studies with 2-(octanesulfonamido)benzoic acid modeled into the active site of squash GPAT revealed an unoccupied volume lined with hydrophobic residues proximal to C-4 and C-5 of the benzoic acid ring. In an effort to produce more potent GPAT inhibitors, a series of 4- and 5-substituted analogs were designed, synthesized, and evaluated for inhibitory activity. In general, compounds containing hydrophobic substituents at the 4- and 5-positions, such as biphenyl and alkylphenyl hydrocarbons, exhibited an improved inhibitory activity against GPAT *in vitro*. The most active compound, 4-([1,1'-biphenyl]-4-carbonyl)-2-(octanesulfonamido)benzoic acid, demonstrated an IC<sub>50</sub> of 8.5 μM and represents the best GPAT inhibitor discovered to date. Conversely, further substitution with hydroxyl or fluoro groups, led to a 3-fold decrease in activity. These results are consistent with the presence of a hydrophobic pocket and may support the binding model as a potential tool for developing more potent inhibitors.

### Introduction

Obesity, defined as having a Body Mass Index (BMI) of 30 or higher, has been implicated in multiple diseases, including cardiovascular disease<sup>1</sup>, type-2 diabetes<sup>2</sup>, hypertension, nonalcoholic fatty liver disease<sup>3</sup>, infertility<sup>4</sup>, and certain types of cancer.<sup>5</sup> According to the World Health Organization, it affects approximately 500 million adults and is the fifth leading risk of deaths globally, accounting for at least 2.8 million deaths a year. Despite an

This journal is © The Royal Society of Chemistry 2013

The Johns Hopkins University, in accordance with its conflict of interest policies, is managing the terms of this arrangement.

†Electronic Supplementary Information (ESI) available: Experimental details including synthetic procedures and characterization data for all novel compounds is available online free of charge. See DOI: 10.1039/b000000x/

increase in obesity and obesity-related diseases, few effective pharmacological therapies currently exist to combat the physiological source of obesity, the accumulation of triacylglycerol (TAG). One approach involves exploiting the mechanisms of the lipid metabolic pathway, either by decreasing the rate of fat synthesis, as shown with the small molecule fatty acid synthase (FAS) inhibitors C75<sup>6</sup> and cerulenin<sup>7</sup>, or increasing the rate of fatty acid oxidation.<sup>8</sup> GPAT catalyzes the transesterification of fatty acyl-CoAs with the primary hydroxyl group of glycerol-3-phosphate (G3P), the first committed and rate-limiting step in the biosynthesis of TAG.<sup>9</sup> In mammals, mitochondrial GPAT (mtGPAT) is an integral membrane protein that co-localizes in the mitochondrion with carnitine-palmitoyl transferase I (CPT1), the rate-limiting enzyme in  $\beta$ -oxidation. These enzymes are co-regulated and compete for fatty acyl-CoA substrates.<sup>10</sup> Inhibition of GPAT by a small molecule inhibitor has the potential to reduce *de novo* synthesis of TAG and to divert the flux of fatty acyl-CoAs to  $\beta$ -oxidation mediated by CPT1, thus making GPAT an attractive therapeutic target against obesity.

Recently, it has been demonstrated that *o*-(alkanesulfonamido)benzoic acids such as **1a-b** (Figure 1) possess moderate inhibitory activity against mammalian GPAT *in vitro*.<sup>11</sup> The 8-carbon derivative **1c** has also been synthesized and exhibits an inhibitory activity comparable to **1b**.<sup>12</sup> The benzoic acid moiety of these compounds, which is deprotonated at physiological pH, is believed to mimic the anionic phosphate group of the native substrate. The relatively acidic aryl sulfonamide hydrogen was proposed to interact with the catalytic histidine responsible for deprotonating the primary hydroxyl group of G3P necessary for acylation. The long alkyl chain of the sulfonamide was designed to bind the lipophilic palmitoyl-CoA binding site.

While structural information regarding mammalian GPAT is limited, X-ray crystal structures of squash GPAT revealed the conserved catalytic HXXXXD motif present in all GPATs as well as a putative G3P binding site comprised of conserved cationic residues Lys193, Arg235, and Arg237.<sup>13a-b</sup> A complex network of relatively hydrophobic pockets and tunnels emanating from the active site was also observed. Protein homology-based modelling of multiple human transferases, including AGPAT1, AGPAT2, and AGPAT9, with the squash GPAT crystal structure showed that, despite low sequence homology, the human transferases are similar in predicted secondary structure and hydrophobic residue distribution.<sup>14</sup> These findings suggest that, although the overall architectures of the acyltransferase homologs differ, structural similarity in the region of the active site may be good. An *in silico* docking simulation of **1c** with squash GPAT, as shown in Figure 2, displayed the inhibitor bound at the putative G3P binding pocket with the carboxylate anion positioned at the phosphate binding site and the long alkyl chain residing in the putative palmitoyl-CoA binding site described by Turnbull *et al.*<sup>13a</sup> Furthermore, the docking model showed a second hydrophobic tunnel, described previously by Tamada *et al.*,<sup>13b</sup> extending away from the G3P binding site and presenting from C-4 and C-5 of the benzoic acid ring of the docked inhibitor. This volume was lined by hydrophobic and aromatic residues including Phe98, Gly99, Tyr102, Ile103, Ala143, Leu176, Pro179, and Phe180.

In an attempt to improve upon the inhibitory activity of **1c**, a series of potential inhibitors was designed and synthesized with various aryl substituents either directly-bound to the 4-

or 5-positions of **1c** or coupled via one of several linkers (keto-, vinyl-, or ethyl-). The aryl substituents were chosen to promote  $\pi$ -stacking with the aromatic residues in the potential hydrophobic channel as well as for synthetic accessibility. The linkers were chosen to examine the effects of pharmacophore separation and conformational rigidity versus flexibility. The 8-carbon chain of **1c** was chosen for its ready commercial availability and, within experimental error, essentially unchanged GPAT inhibitory activity compared to the nonyl side chain reported previously.<sup>11</sup> The candidates were tested for GPAT inhibition *in vitro* to develop a structure-activity relationship and assess the validity of the docking model as a tool to direct future medicinal chemistry efforts.

## Results and Discussion

### Synthesis of 4- and 5-substituted Analogs

An efficient, divergent route was devised to access the 4- and 5-substituted derivatives of **1c**. Sulfonamide coupling of 4- and 5-bromoantranilates **2** and **3**, respectively, with octanesulfonyl chloride generated sulfonamides **4** and **5**. Suzuki-Miyaura coupling reactions with various aryl boronic acids were then performed either under argon to afford coupling products **6a–l** and **7a–l** or under an atmosphere of carbon monoxide to afford keto-linker precursors **8a–b** and **9a–d**. Alternatively, coupling of **4** and **5** with various *trans*-arylvinyl boronic acids under an argon atmosphere provided vinyl-linker precursors **10a–b** and **11a–b**. Each of the benzoates was then hydrolyzed, either under Gassman conditions<sup>15</sup> or in aqueous 1 M NaOH, to afford analogs **12a–l**, **13a–l**, **14a–b**, **15a–d**, **16a–b** and **17a–b**. Alternatively, hydrogenation of **10a–b** and **11a–b** prior to hydrolysis afforded ethyl-linked analogs **18a–b** and **19a–b**.

### Inhibition Data

The inhibitory data for the 4-aryl-substituted analogs are presented in Table 1. Several of these compounds exhibited marked improvement over **1c**. In general, hydrophobic substituents such as *p*-*n*-butylphenyl (**12d**), biphenyl (**12e,f**), and methoxyphenyl (**12g,h**) exhibited a moderate increase in inhibitory activity of up to 2-fold. Chlorophenyl analogs (**12a–c**) also demonstrated markedly more potent inhibition, particularly the *meta*-chloro analog which also was about 2-fold more active than **1c**. Conversely, hydroxyl- and fluoro-containing analogs (**12i–l**) caused a modest decrease in inhibitory activity. The *para*-hydroxyl analog, for instance, showed a nearly 3-fold decline in inhibition.

The inhibitory data for the 5-aryl analogs is presented in Table 2. Generally, the structure-activity relationship of this class mirrors that of the 4-aryl class. For instance, several of the compounds showed notable improvement over **1c**, particularly those containing chlorophenyl and hydrophobic substituents. Specifically, both the *meta*-chloro (**13b**) and *para*-*n*-butyl (**13d**) analogs effected a 2.9-fold increase in inhibitory activity. Also similar to the 4-aryl class, hydroxyphenyl and fluorophenyl groups were not well tolerated, decreasing inhibition by nearly 3-fold.

The data for the 4- and 5-aryl analogs are consistent with the presence of a hydrophobic binding pocket extending from C-4 and C-5 of the benzoic acid of **1**. Both steric and

electronic factors may be affecting binding in this pocket. Sterically, the pocket is large enough around the 4-position of **1c** to accommodate the relatively voluminous and rigid *ortho*- and *para*-biphenyl analogs **12e** and **12f**. The region near the 5-position, however, appears more constrained in size. Consequently, the *para*-biphenyl analog **13f** shows a large decrease in activity, possibly due to steric interactions with residues on the edge of the binding pocket. The *ortho*-biphenyl analog **13e**, however, may orient the terminal phenyl substituent away from the edge and back into the binding pocket resulting in a 2.5-fold increase in activity. Van der Waals and  $\pi$ -stacking interactions seem to be favored within the pocket as phenyl-, alkylphenyl-, and alkoxyphenyl substituents showed an increase in activity. Conversely, the more polarized fluorine-containing analogs demonstrated moderately diminished activity possibly due to binding at a site intolerant of the inhibitor's high charge density or disruption of key  $\pi$ - $\pi$  interactions within the hydrophobic channel.

While the 3-fold increase in observed activity for the 4-aryl and 5-aryl derivatives was promising, we worried that the kinked nature of the hydrophobic tunnel observed in the docking model was preventing the analogs from extending fully into it. Therefore, we next sought to incorporate various linker regions on a subset of the more promising hydrophobic leads. Keto, vinyl, and ethyl linkers were chosen to examine the effect of separating the substituents from the pharmacophore and to explore conformational rigidity versus flexibility in extending the substituents into the hydrophobic tunnel. Inhibition data for the 4- and 5-substituted analogs are shown in Table 3 and Table 4, respectively. In general, the analogs possessing a keto linker were slightly to moderately less potent than the corresponding structures without a linker. For example, 5-keto-substituted *para-n*-butyl analog **15a** exhibited a 3.5-fold decrease in inhibition compared to compound **13d**. The *para*-biphenyl analogs **14b** and **15b**, however, were notable exceptions. Compound **14b** showed a 2-fold more potent inhibition compared to the linker-free analog **13f**. While the rigid linear carbon skeleton of **13f** may sterically interfere with residues on the face of the hydrophobic pocket, the ketone linker in **15b** could potentially direct the large biphenyl moiety back towards the cavity. Compound **14b**, with an  $IC_{50}$  of 8.5  $\mu$ M, was 3-fold more potent than **1c** and, to our knowledge, represents the most active GPAT inhibitor discovered to date.

The rigid vinyl and conformationally-flexible ethyl linkers were generally not well tolerated. For example, **16b**, a vinyl-linked *para*-methoxyphenyl analog, produced an activity of 37.5  $\mu$ M compared to 13.3  $\mu$ M for the linker-free derivative **12h**. No significant benefit was apparent from the incorporation of the conformationally-flexible ethyl linkers. The same *para*-methoxyphenyl substituent with a linker region in compound **18b** demonstrated an  $IC_{50}$  of 43.0  $\mu$ M or 3.2-fold lower activity than the corresponding compound **12h**.

## Conclusions

Several 4- and 5-substituted analogs of GPAT inhibitor (octanesulfonamido)benzoic acid were synthesized and analyzed for *in vitro* inhibitory activity. In general, hydrophobic substituents led to an increase in inhibitory activity while more polar and hydrogen-bonding substituents showed a decrease in inhibitory activity, consistent with the presence of a hydrophobic pocket identified by *in silico* studies. Taking advantage of the hydrophobic

pocket, *p*-biphenylketone-substituted **14b** improved the inhibitory activity 3-fold to 8.5  $\mu\text{M}$ , representing the most potent GPAT inhibitor to date. Future studies will aim to determine whether further extension of aryl and alkyl substituents into this channel confers additional inhibitory activity and if the observed increases *in vitro* correlate with *in vivo* TAG biosynthesis and overall fat metabolism in keeping with earlier studies.<sup>16</sup>

## Supplementary Material

Refer to Web version on PubMed Central for supplementary material.

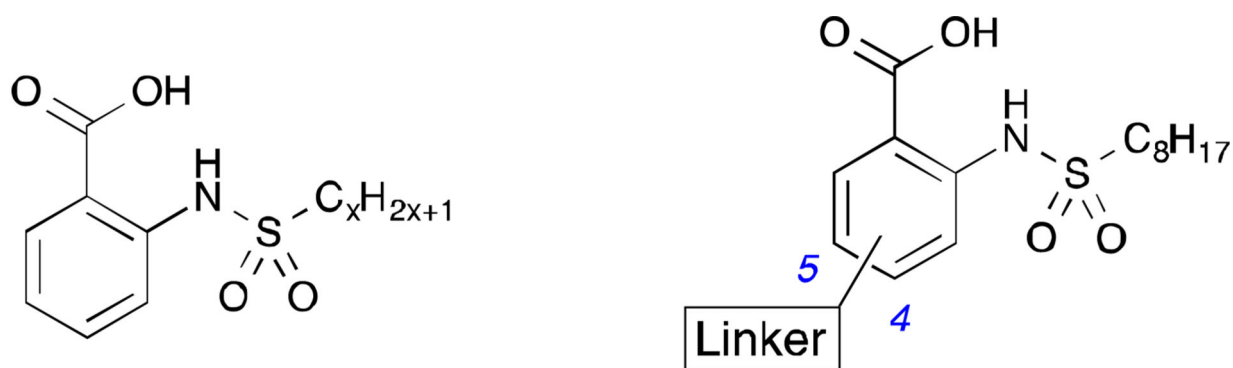
## Acknowledgments

We would like to thank Dr. I. P. Mortimer for performing HRMS analyses. This work was supported by the NIH 1R43DK65423 to FASgen, Inc. Under a license agreement between FASgen, Inc. and The Johns Hopkins University, C.A.T. is entitled to share royalty received by the University on sales of products described in this article. C.A.T. owns FASgen, Inc. stock, which is subject to certain restrictions under university policy.

## Notes and references

1. a) Poirier P, Giles TD, Bray GA, et al. *Arterioscler. Thromb. Vasc. Biol.* 2006; 26:968–976. [PubMed: 16627822] b) Bastien M, Poirier P, Lemieux I, Després J-P. *Prog. Cardiovasc. Dis.* 2014; 56:369–381. [PubMed: 24438728]
2. Haslam DW, James WP. *Obesity. Lancet.* 2005; 366:1197–1209. [PubMed: 16198769]
3. a) Hall JE. *Hypertension.* 2003; 41:625–633. [PubMed: 12623970] b) Adams ST, Salhab M, Hussain ZI, Miller GV, Leveson SH. *Blood Pressure.* 2013; 22:131–137. [PubMed: 23244451]
4. Hammoud AO, Gibson M, Peterson CM, Meikle AW, Carrell DT. *Fertil. Steril.* 2008; 90:897–904. [PubMed: 18929048]
5. a) Calle EE, Rodriguez C, Walker-Thurmond K, Thun MJ. *N. Engl. J. Med.* 2003; 348:1625–1638. [PubMed: 12711737] b) Pantasri T, Norman RJ. *Gynecol. Endocrinol.* 2014; 30:90–94. [PubMed: 24188449]
6. a) Loftus TM, Jaworski DE, Frehywot GL, Townsend CA, Ronnett GV, Lane MD, Kuhajda FP. *Science.* 2000; 288:2379–2381. [PubMed: 10875926] b) Gilbert CA, Slingerland JM. *Annu. Rev. Med.* 2013; 64:45–57. [PubMed: 23121183]
7. Makimura H, Mizuno TM, Yang XJ, Silverstein J, Beasley J, Mobbs CV. *Diabetes.* 2001; 50:733–739. [PubMed: 11289036]
8. Thupari JN, Landree LE, Ronnett GV, Kuhajda FP. *Proc. Natl. Acad. Sci. U.S.A.* 2002; 99:9498–9502. [PubMed: 12060712]
9. Coleman RA, Lewin TM, Muoio DM. *Annu. Rev. Nutr.* 1998; 18:331–351. [PubMed: 9706228]
10. Muoio DM, Seefeld K, Witters LA, Coleman RA. *Biochem. J.* 1999; 338(Pt 3):783–791. [PubMed: 10051453]
11. Wydysh EA, Medghalchi SM, Vadlamudi A, Townsend CA. *J. Med. Chem.* 2009; 52:3317–3327. [PubMed: 19388675]
12. See Supplemental Information for the synthetic protocol to compound **1c**
13. a) Turnbull AP, Rafferty JB, Sedelnikova SE, Slabas AR, Schierer TP, Kroon JT, Simon JW, Fawcett T, Nishida I, Murata N, Rice DW. *Structure.* 2001; 9:347–353. [PubMed: 11377195] b) Tamada T, Feese MD, Ferri SR, Kato Y, Yajima R, Toguri T, Kuroki R. *Acta Crystallogr D Biol Crystallogr.* 2003; 60:13–21. [PubMed: 14684887]
14. Agarwal AK, Sukumaran S, Bartz R, Barnes RI, Garg A. *Journal of Endocrinology.* 2007; 193:445–457. [PubMed: 17535882]
15. Gassman PG, Schenk WN. *J. Org. Chem.* 1977; 42:918–920.

16. Kuhajda FP, Aja S, Tu Y, Han WF, Medghalchi SM, Meskini EI R, Landree LE, Peterson JM, Daniels K, Wong K, Wydysh EA, Townsend CA, Ronnett GV. *Am. J. Physiol. Regul. Integr. Comp. Physiol.* 2011; 301:R116–R130. [PubMed: 21490364]



**1a** ( $x = 16$ )  $IC_{50} = 18.3 \pm 1.9 \mu\text{M}$

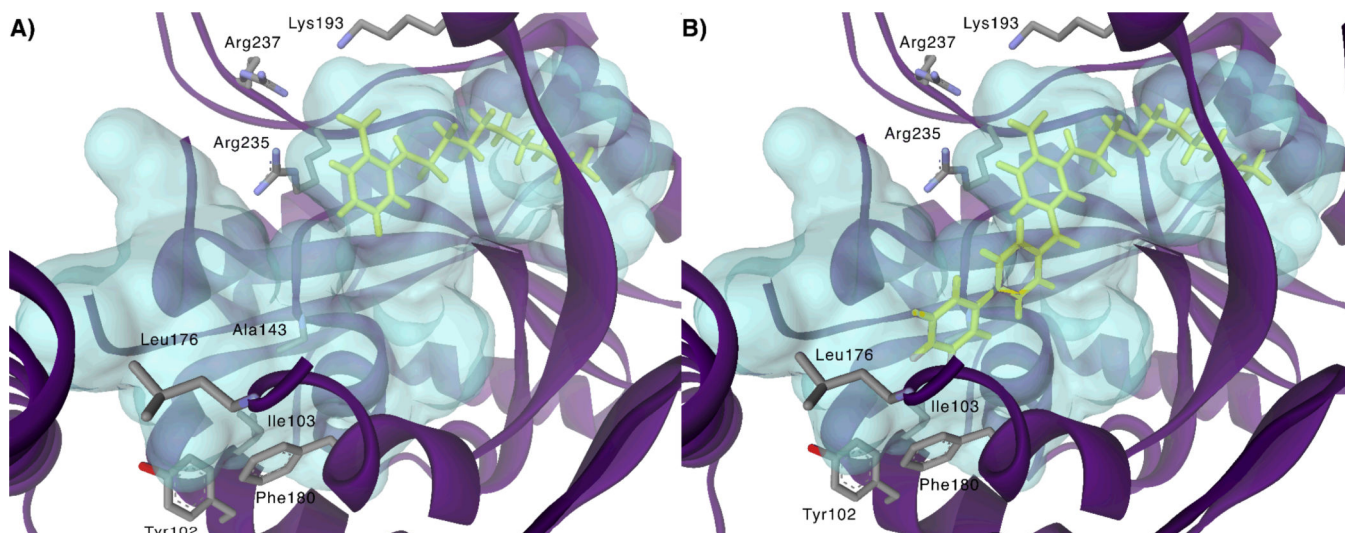
**1b** ( $x = 9$ )  $IC_{50} = 24.7 \pm 2.1 \mu\text{M}$

**1c** ( $x = 8$ )  $IC_{50} = 25.7 \pm 2.4 \mu\text{M}$

Ar

Linker = none, keto-,  
vinyl-, ethyl-

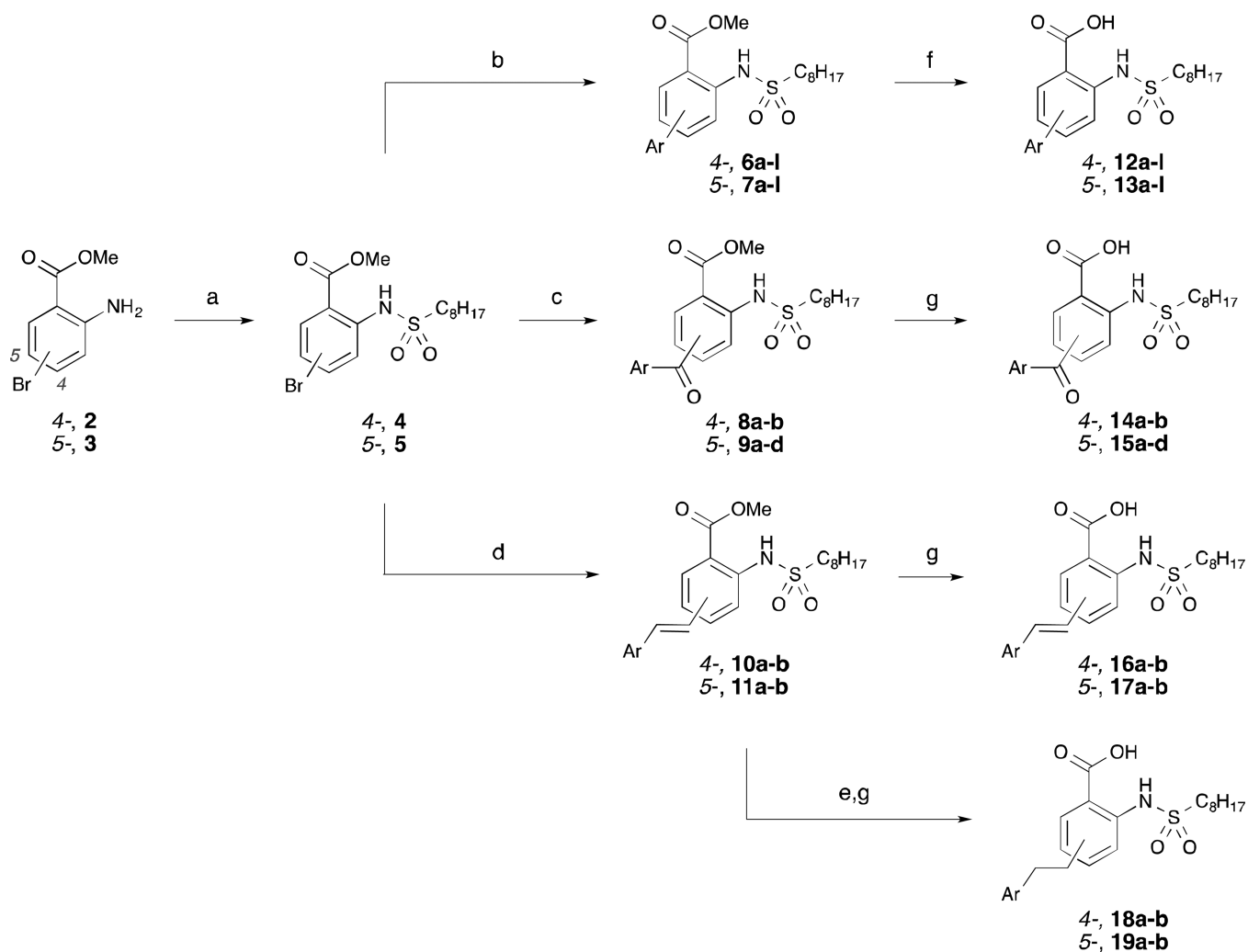
**Figure 1.**  
Structure of *o*-(alkanesulfonamido)benzoic acid GPAT inhibitors (**1a–c**) and proposed  
analogs



**Figure 2.**

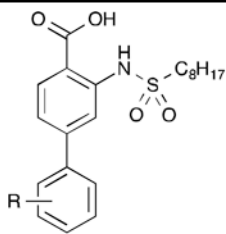
A) Compound **1c** (yellow) docked into the active site of squash GPAT using the CDOCKER protocol with Accelrys Discovery Studio (version 2.1). B) Compound **14b** manually docked into the binding site obtained for compound **1c**.



**Scheme 1.**

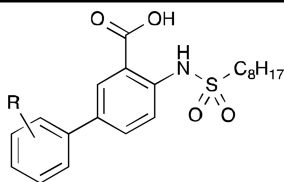
*Reagents and Conditions:* a) ClSO<sub>2</sub>C<sub>8</sub>H<sub>17</sub>, NEt<sub>3</sub>, CH<sub>2</sub>Cl<sub>2</sub>, 62–76%; b) Pd(PPh<sub>3</sub>)<sub>4</sub>, Ar-B(OH)<sub>2</sub>, Na<sub>2</sub>CO<sub>3</sub>, PhMe/MeOH, 90 °C, 45–80%; c) Pd(PPh<sub>3</sub>)<sub>4</sub>, Ar-B(OH)<sub>2</sub>, K<sub>2</sub>CO<sub>3</sub>, dioxane, 90 °C, CO (1 atm), 28–46%; d) Pd(PPh<sub>3</sub>)<sub>4</sub>, (E)-Ar-(CH)<sub>2</sub>B(OH)<sub>2</sub>, K<sub>2</sub>CO<sub>3</sub>, PhCH<sub>3</sub>, 105 °C, 58–83%; e) Pd/C, H<sub>2</sub> (1 atm), MeOH, 80–91%; f) KOtBu, H<sub>2</sub>O, Et<sub>2</sub>O, 0 °C-r.t., 71–94%; g) 1 M NaOH, THF, 40 °C, 73–92%.

Table 1

GPAT Inhibition by 4-Substituted Derivatives<sup>a</sup>

Compound	R	IC <sub>50</sub> (μM) ± SD
12a	<i>o</i> -Cl	26.9 ± 4.1
12b	<i>m</i> -Cl	13.8 ± 2.5
12c	<i>p</i> -Cl	18.1 ± 3.5
12d	<i>p-n</i> -C <sub>4</sub> H <sub>9</sub>	15.7 ± 1.6
12e	<i>o</i> -C <sub>6</sub> H <sub>5</sub>	17.1 ± 0.8
12f	<i>p</i> -C <sub>6</sub> H <sub>5</sub>	13.5 ± 3.2
12g	<i>o</i> -OCH <sub>3</sub>	16.1 ± 0.5
12h	<i>p</i> -OCH <sub>3</sub>	13.3 ± 1.1
12i	<i>o</i> -F	47.2 ± 2.0
12j	<i>m</i> -F	32.6 ± 3.6
12k	<i>o</i> -OH	63.1 ± 5.5
12l	<i>p</i> -OH	64.8 ± 3.8

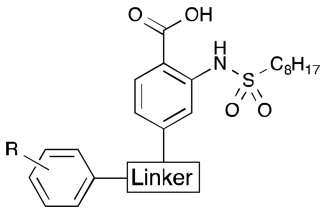
<sup>a</sup> A description of assay conditions can be found in the Supplemental Information.

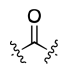
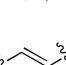
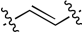
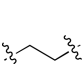
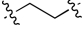
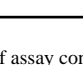
**Table 2**GPAT Inhibition by 5-Substituted Derivatives<sup>a</sup>

Compound	R	IC <sub>50</sub> (μM) ± SD
<b>13a</b>	<i>o</i> -Cl	14.4 ± 1.3
<b>13b</b>	<i>m</i> -Cl	8.9 ± 0.9
<b>13c</b>	<i>p</i> -Cl	9.2 ± 0.7
<b>13d</b>	<i>p</i> - <i>n</i> -C <sub>4</sub> H <sub>9</sub>	9.0 ± 0.4
<b>13e</b>	<i>o</i> -C <sub>6</sub> H <sub>5</sub>	10.1 ± 0.7
<b>13f</b>	<i>p</i> -C <sub>6</sub> H <sub>5</sub>	29.1 ± 6.3
<b>13g</b>	<i>o</i> -OCH <sub>3</sub>	27.6 ± 2.0
<b>13h</b>	<i>p</i> -OCH <sub>3</sub>	19.5 ± 5.5
<b>13i</b>	<i>o</i> -F	34.6 ± 2.0
<b>13j</b>	<i>m</i> -F	37.6 ± 9.7
<b>13k</b>	<i>o</i> -OH	61.7 ± 13.8
<b>13l</b>	<i>p</i> -OH	47.3 ± 6.4

<sup>a</sup> A description of assay conditions can be found in the Supplemental Information.

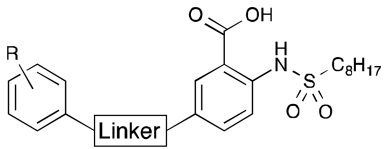
Table 3

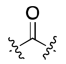


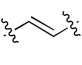

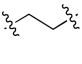
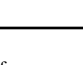
4-Substituted Inhibitors with Linkers<sup>a</sup>


Compound	Linker	R	IC <sub>50</sub> (μM)
14a		<i>p</i> - <i>n</i> -C <sub>4</sub> H <sub>9</sub>	15.8±0.8
14b		<i>p</i> -C <sub>6</sub> H <sub>5</sub>	8.5±2.1
16a		-H	38.0±9.9
16b		<i>p</i> -OCH <sub>3</sub>	38.7±6.3
18a		-H	37.5±4.8
18b		<i>p</i> -OCH <sub>3</sub>	43.0±9.3

<sup>a</sup> A description of assay conditions can be found in the Supplemental Information.

Table 4

5-Substituted Inhibitors with Linkers<sup>a</sup>


Compound	Linker	R	IC <sub>50</sub> (μM)
15a		<i>p</i> - <i>n</i> -C <sub>4</sub> H <sub>9</sub>	31.7±3.2
15b		<i>p</i> -C <sub>6</sub> H <sub>5</sub>	13.0±0.6
15c		<i>o</i> -OCH <sub>3</sub>	59.2±3.8
15d		<i>p</i> -OCH <sub>3</sub>	44.3±9.2
17a		-H	16.3±5.3
17b		<i>p</i> -OCH <sub>3</sub>	37.1±8.3
19a		-H	37.5±4.8
19b		<i>p</i> -OCH <sub>3</sub>	26.3±2.4

<sup>a</sup> A description of assay conditions can be found in the Supplemental Information.